Experimental parameters for a reactor antineutrino experiment at very short baselines

K. M. Heeger and M. N. Tobin

Department of Physics, University of Wisconsin, Madison, Wisconsin 53706, USA

B. R. Littlejohn*

Physics Department, University of Cincinnati, Cincinnati, Ohio 45221, USA

H. P. Mumm

National Institute of Standards and Technology, Gaithersburg, Maryland 20899, USA

Reactor antineutrinos are used to study neutrino oscillation, search for signatures of nonstandard neutrino interactions, and monitor reactor operation for safeguard applications. The flux and energy spectrum of reactor antineutrinos can be predicted from the decays of the nuclear fission products. A comparison of recent reactor calculations with past measurements at baselines of 10–100 m suggests a 7.2% deficit. Precision measurements of reactor antineutrinos at very short baselines $\mathcal{O}(1$–10 m) can be used to probe this anomaly and search for possible oscillations into sterile neutrino species. This paper studies the experimental requirements for a new reactor antineutrino measurement at very short baselines and calculates the sensitivity of various scenarios. We conclude that, given proper site optimization, detector design, and background reduction, an experiment at a typical research reactor can provide 5σ discovery potential for the favored oscillation parameter space with 3 years of detector live time.

I. INTRODUCTION

Recent calculations of the predicted $\bar{\nu}_e$ flux from reactors [1] compared to past measurements at baselines between 10 and 100 m have revealed a 7.2% deficit, an effect with a significance of 3σ confidence level [2]. This discrepancy, the *reactor anomaly*, can be interpreted as a sign of new physics or point to an issue with the reactor flux calculations [3]. Independent calculations have verified the reactor $\bar{\nu}_e$ flux predictions [4], but subsequent calculations based on a full *ab initio* prediction using newly available nuclear data [5] reduce the size of the discrepancy. It has been suggested that the reactor anomaly may be the signature of additional sterile neutrino states with mass splittings of the order of ~ 1 eV^2 and oscillation lengths of $\mathcal{O}(3$ m) [6,7]. Other anomalies in neutrino physics including the observation of apparent ν_e and $\bar{\nu}_e$ appearance at similar mass-squared splittings in accelerator experiments [8–11], deficits in observed events from high-intensity ν_e sources used to calibrate solar neutrino detectors [12,13], and the preference for more than three relativistic species in astrophysical surveys [14,15] add to the puzzle.

Additional data will soon be provided by the currently operating kilometer-scale reactor experiments, Daya Bay, Double Chooz, and RENO [16–18]. While highly precise, these experiments cannot resolve the short oscillation lengths associated with eV^2 mass splittings; at these distances and with a finite detector energy resolution, the oscillation effect from potential sterile states averages to

yield an effective rate deficit. Moreover, these measurements will eventually be limited by the understanding of the interference of multiple reactor cores, the presence of oscillation effects from other mass-squared splittings, and the inability to take background data free of reactor $\bar{\nu}_e$. A new experiment at very short (< 10 m) baselines with a single core in a controlled research environment where backgrounds can be measured independently is needed to fully disentangle reactor flux and spectrum prediction uncertainties from sterile neutrino oscillation effects or other signs of new physics.

This paper explores some of the experimental requirements of a very-short-baseline experiment at reactors and the related sensitivity to oscillation parameters. The paper is organized as follows: Section II summarizes both the experimental detector and reactor parameters under consideration. Section III introduces the characteristic signature of neutrino oscillations and defines the χ^2 analysis used to calculate experimental sensitivity. A nominal, generic reactor-detector arrangement referred to as the "default experiment" is defined for systematic studies and comparison. Sections IV, V, VI, and VII present a discussion of reactor, facility, background, and detector parameters and examine the impact on the overall sensitivity of the experiment. Section VIII summarizes the sensitivity and discovery potential of a new reactor experiment and discusses its optimization.

II. EXPERIMENTAL PARAMETERS

A number of experiments have been proposed to address the reactor anomaly by making a precise measurement of the reactor flux and spectrum at very short baselines

---

*littlebh@uc.edu

[19–23]. The proposed experimental configurations are site specific and reflect the infrastructure and logistical constraints at each site. This work studies generic experimental parameters that determine the ultimate sensitivity of a reactor experiment at very short baselines and helps guide the optimization of a new experiment aimed at a definitive sterile neutrino oscillation search.

A. Reactor parameters

Antineutrinos from the reactor core are used as the flavor-pure $\bar{\nu}_e$ source. The relevant reactor core parameters are the following:

(I) *Reactor power.*—Each nuclear fission initiates the release of a known amount of energy along with several antineutrinos. The reactor $\bar{\nu}_e$ flux is proportional to the thermal power output of the reactor modulo corrections for the isotopic fuel composition. High operating power combined with high reactor up time maximizes the event statistics. Most commercial reactors, but not all research reactors, operate close to their licensed power.

(II) *Fuel type.*—Most nuclear reactors utilize uranium-based fuel containing a mixture of ^{238}U and ^{235}U, with the latter providing the majority of total fissions and thermal power. The two most common classes of reactor fuels, commercial and highly enriched, differ primarily in their ^{235}U fission fractions. Highly enriched uranium (HEU) fuel, commonly utilized in research reactors, contains 90% or more ^{235}U, with fission fractions dominated by ^{235}U at all points in the fuel cycle. Commercial fuel generally contains less than 6% ^{235}U. While ^{235}U fission comprises the majority of all fissions in these cores, a significant fraction (30%–50%, depending on the fuel burnup) is contributed by ^{238}U and by ^{239}Pu and ^{241}Pu accumulated during the fuel cycle [24]. These isotopes produce different proportions of fission products, resulting ultimately in a difference in the total number, energy spectrum, and spectral uncertainty of produced $\bar{\nu}_e$.

(III) *Duty cycle.*—The duty cycle is given by the ratio of the power cycle to the subsequent shutdown periods for refueling or maintenance. The duty cycle influences the statistical power of an experiment. Throughout this paper, we present results only in terms of detector live time. Reactor down time can be used for determining the energy spectrum and position distribution of cosmogenic and some reactor-related backgrounds [25–27].

(IV) *Core dimensions.*—Antineutrinos are produced throughout the active reactor core and emitted isotropically. The core's finite dimensions cause a spread in the neutrino path lengths between the reactor core and detector that washes out the observable oscillation in the detector.

As examples, we use parameters from three research reactors in the United States, the High Flux Isotope Reactor (HFIR) at Oak Ridge National Laboratory [28], the National Bureau of Standards Reactor at National Institute of Standards and Technology (NIST) [29], and the Advanced Test Reactor (ATR) at Idaho National Laboratory [30]. The Institut-Laue Langevin (ILL) reactor in France and the commercial San Onofre Nuclear Generating Station (SONGS) in California are included for reference [31,32].

B. Facility parameters

The reactor facility provides constraints on the location of the detector, its size, and distance to the core. The following parameters determine an experiment's design and sensitivity:

(I) *Experimental space and detector volume.*—Detector location, geometry, and dimensions are limited by the available space near the reactor core. Typically, biological shielding limits the distance of closest approach to the reactor, while the cross-sectional area of the detector and the maximum radial distance are constrained by the layout of the reactor facility, floor-loading limits, and the availability of floor space not occupied by other experiments, reactor equipment, or detector shielding. To maximize event statistics, a large cross-sectional area at close radial distances is desirable.

(II) *Detector distance to core.*—The closest distance to the reactor determines the overall $\bar{\nu}_e$ flux seen by the detector as well as the oscillation wavelength probed. For the following discussion we define this distance of closest approach, r_{min}, to be from the center of the reactor core to the closest point in the active detector target.

Throughout this discussion we explore a range of detector sizes and closest distances reflecting the expected space available at U.S. facilities.

C. Detector parameters

Intrinsic detector characteristics determine the observed event distributions:

(I) *Fiducial volume and target mass.*—The observed number of $\bar{\nu}_e$ interactions in the detector scales with the number of target protons in the detector and sets the statistical precision of the experiment.

(II) *Detection efficiency.*—The detection efficiency is determined by many factors, such as cosmic muon rates and veto window length, amount of nonscintillating material in the target volume, low-energy analysis threshold, and spatial compactness and energy of the delayed inverse beta signals in the detector. Efficiency directly scales the detected number of events. For fixed signal-to-background (S/B), changes in the detection efficiency have the

same effect as increasing the detector volume or target mass.

(III) *Position and energy resolution.*—An unambiguous demonstration of neutrino oscillation requires the observation of oscillations in energy and distance, the characteristic L/E dependence. Good position and energy resolution are necessary to maximize the experimental sensitivity.

D. Backgrounds

A reactor experiment at very short baseline from a reactor requires the operation of a detector on the surface under minimal overburden. Muon and cosmic ray-induced backgrounds as well as backgrounds from the reactor are thus very important considerations. Cosmic backgrounds consist of muons and their associated spallation products, as well as hadronic cosmic rays. Reactor-correlated backgrounds at such short baselines will be significant and will consist of fast and thermal neutrons created in the fission process, as well as high-energy gamma rays created by neutron activation of surrounding materials, such as cooling water, shielding, and metal infrastructure surrounding the core. Small but irreducible backgrounds similar in energy spectrum to the signal may also be provided by spent nuclear fuel nearby the reactor [33]. Both the magnitude and spectral characteristics of backgrounds are expected to be highly site specific, depending on many variables such as experimental depth and surrounding building structures, distance from the reactor, reactor power, detector and reactor shielding, and proximity of the detector to reactor cooling and other infrastructure.

The effect of backgrounds on the sensitivity of a very-short-baseline (VSBL) experiment are investigated in this paper by considering variations in key background metrics based on current R&D efforts at VSBL reactor experiments [20] and experience from previous reactor experiments [27,31,34]. Detailed site-specific background studies at U.S. research reactors are currently underway and are thus not discussed in this paper. This paper can provide guidance to these R&D efforts by determining the background requirements that must be achieved for a sufficiently sensitive experimental arrangement. These future R&D efforts can then decide which techniques (i.e., some combination reactor on-off background subtraction, active shielding, segmentation, pulse shape discrimination, etc.) will be utilized to try to meet these requirements.

Specifically, this paper considers the following background parameters:

(I) *Signal-to-background ratio.*—The overall S/B ratio is a measure of the total magnitude of time-coincident backgrounds and accidental background in the delayed coincidence window of the inverse beta-decay reaction at all energies and positions. The choice of analysis low-energy threshold, which can be raised or lowered in response to observed S/B rates at low energies, will also be investigated.

(II) *Background spectral shape.*—The backgrounds' energy dependence will determine the measured spectral shape of the observed events. Energy-dependent background subtraction and/or fitting will be important for the analysis of the energy-dependent oscillation signature.

(III) *Background position distribution.*—In the vicinity of a reactor significant spatial variations of backgrounds are expected. In particular, fast neutrons can scatter from surrounding materials, building structures, and even other experiments. Measurement of the observed event rate as a function of position through detector movement or segmentation will be critical for understanding local background variations on the meter scale.

III. EXPERIMENTAL SIGNATURE

A. Oscillations of reactor antineutrinos

Antineutrinos from reactors are produced as flavor-pure $\bar{\nu}_e$ in the decays of neutron-rich fission products in the reactor fuel. More than 99.9% of all $\bar{\nu}_e$ emitted from commercial reactors are produced within the decay chains of four isotopes: ^{235}U, ^{238}U, ^{239}Pu, and ^{241}Pu. The thermal heat released in the nuclear decays is proportional to the number of emitted $\bar{\nu}_e$ and is thus a measure of the flux of expected antineutrinos. The spectrum of reactor antineutrinos detected via inverse beta decay has a mean energy of about 4 MeV and extends up to roughly 10 MeV.

Neutrinos and antineutrinos are produced as a linear combination of mass eigenstates and their flavor is associated with the accompanying lepton. Due the difference in the mass eigenstates the flavor of observed neutrinos oscillates as a function of baseline and energy. For the three active neutrino states the neutrino mixing parameters are well measured in atmospheric, solar, reactor, and accelerator based experiments. Reactor $\bar{\nu}_e$ disappearance over baselines of 1–2 km and $\sim$180 km has been observed [16–18,35]. The oscillation probability can be parametrized in terms of the mass splitting Δm_{ij}^2 and the mixing angle θ_{ij} between the ith and jth mass eigenstates. Additional sterile neutrino mass states with $\Delta m^2 \sim 1$ eV^2 beyond the three active neutrinos would yield an oscillation effect over meter-long baselines with survival probability described by

$$P_{\mathrm{sur}}(E, \vec{L}) \simeq 1 - \sin^2 2\theta_{ee} \sin^2\left(\frac{1.27\Delta m_{41}^2 |\vec{L} - \vec{r}|}{E}\right) \quad (1)$$

with oscillation parameters Δm_{41}^2 and $\sin^2 2\theta_{ee}$.

Figure 1 illustrates the oscillation effect in baseline and energy for ($\Delta m^2 = 1.8$ eV^2, $\sin^2 2\theta_{ee} = 0.5$). The characteristic L/E oscillation is pictured in Fig. 2 for the sterile neutrino oscillation parameters (1.8 eV^2, 0.1) preferred in global fits [6] and the default experimental arrangement described below.
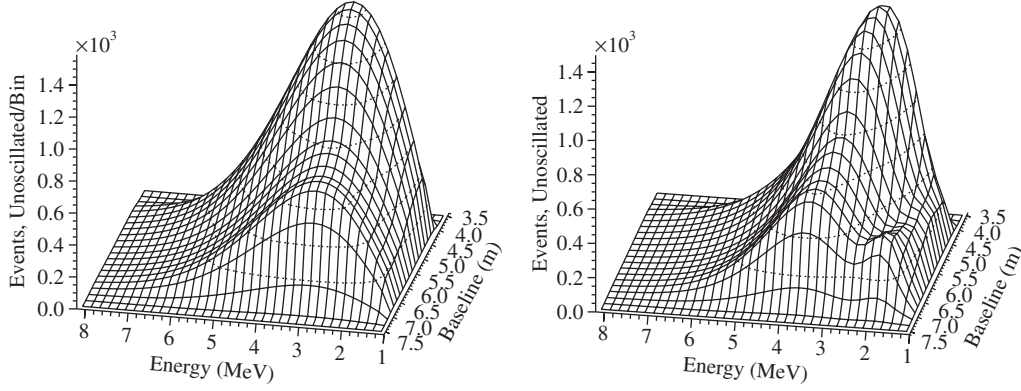
FIG. 1.   Unoscillated (left) versus oscillated (right) detected $\bar{\nu}_e$ spectra at ($\Delta m^2 = 1.8$ eV^2, $\sin^2 2\theta_{ee} = 0.5$) for a reactor $\bar{\nu}_e$ detector with realistic parameters as described in Table I. Exaggerated oscillation values are chosen for illustrative purposes. The change in spectral shape from baseline to baseline is a key signature of neutrino oscillations.

B. A nominal reactor antineutrino experiment at very short baselines

Reactor neutrino experiments typically utilize the inverse beta decay reaction $\bar{\nu}_e + p \rightarrow e^+ + n$ with a threshold of ~ 1.8 MeV to measure the flux and energy spectrum of reactor $\bar{\nu}_e$. Liquid scintillating (LS) detectors provide a proton-rich target with high detection efficiency and good energy resolution. Energy resolutions of around 8% and total detection efficiencies of 75%–85% have been obtained in recent large-scale underground experiments [16,17]. For smaller detectors developed for early short-baseline $\bar{\nu}_e$ experiments and more recent reactor monitoring purposes, energy resolutions of 10%–20% and efficiencies of 10%–50% have

been reported [27,36–38]. Rejection of backgrounds can be achieved by the tried-and-true methods of time coincidence and rejection of muon-correlated triggers, as well as by other previously demonstrated methods of selection based on event topology and pulse shape discrimination. For the studies presented in this paper a nominal experimental arrangement of a $\mathcal{O}(1$ m$^3)$-sized detector at distances of $\mathcal{O}(10$ m) from an average research reactor is considered. The specific parameters utilized in this nominal arrangement are listed in Table I.

C. Experimental sensitivity and discovery potential

The sensitivity of a reactor experiment to neutrino oscillations is evaluated by comparing the detected energy spectrum to the expected one in the absence of neutrino oscillations. A radially extended detector with position resolution allows a comparison as a function of baseline. A χ^2 test is used to test the hypothesis of no oscillation and for parameter estimation in Δm_{41}^2 and $\sin^2 2\theta_{ee}$. Observed $\bar{\nu}_e$ events are binned in energy E with index i and in distance between the core and the point of detection, $|\vec{L}|$, along index j. The expected unoscillated number of events per bin, T_{ij}, is given by

$$T(E, \vec{L}) = \frac{N_p \epsilon}{4\pi} \int \frac{\sigma(E) S(E)}{|\vec{L} - \vec{r}|^2} d\vec{r} \qquad (2)$$

with N_p as the number of target protons, the detection efficiency ϵ, energy E, point vector $\vec{r}$ between the core center and $\bar{\nu}_e$ production point in the core, vector $\vec{L}$ between the core center and $\bar{\nu}_e$ detection point in the detector, $\bar{\nu}_e$ energy spectrum $S(E)$, and inverse beta cross section $\sigma(E)$. M_{ij} is the expected number T_{ij} with backgrounds added in the presence of sterile neutrino oscillations as described by Eq. (1). Both M_{ij} and T_{ij} are subject to Gaussian position and energy resolution smearing according to the values given in Table I. The χ^2 function is defined as
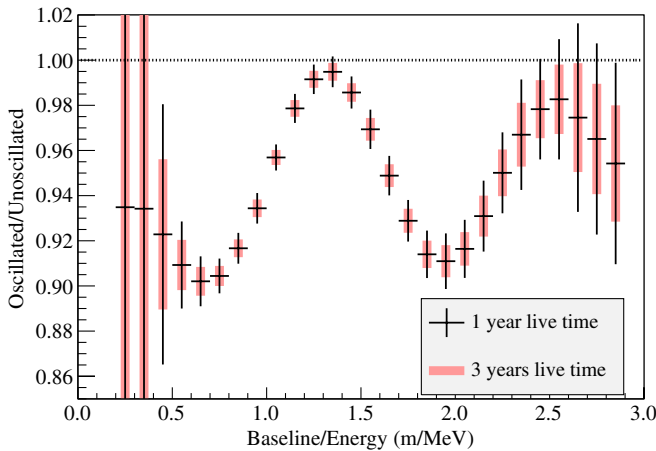

FIG. 2 (color online).   Ratio of the oscillated to unoscillated spectrum as a function of L/E for ($\Delta m^2 = 1.8$ eV^2, $\sin^2 2\theta_{ee} = 0.1$) and the nominal experimental arrangement described in Sec. III B. One year of live time provides 220 000 signal events. With the nominal 30% detection efficiency and example reactor up times provided by NIST, such statistics can be achieved in approximately 1.5 years of calendar time. Error bars are purely statistical.

TABLE I. Nominal experimental parameters used for the sensitivity calculations presented in this paper.

	Parameter	Value	Comment	Reference
Reactor	Power	20 MW	NIST-like	[39]
	Shape	Cylindrical	NIST-like	[39]
	Size	0.5 m radius, half-height	NIST-like	[39]
	Fuel	HEU	Research reactor fuel type	[39–41]
	Dimensions	$1 \times 1 \times 3$ m	3 meters of available baseline	$\cdots$
Detector	Efficiency	30%	In range of SBL exps. (10%–50%)	[27,36,37,42]
	Proton density	$6.39 \times 10^{28} \frac{p}{m^3}$	In range of LS exps	[43]
	Position resolution	15 cm	Daya Bay-like	[34]
	Energy resolution	$10\%/\sqrt{E}$	Daya Bay-like	[44]
	S/B ratio	1	In range of SBL exps. (1–25)	[27,31,36]
Background			In range of VSBL R&D (1)	[42]
	Background shape	$1/E^2$ + Flat	Low-energy accidentals ($1/E^2$) Neutron bkg (flat approximation)	$\cdots$
Other	Run time	1 year live time	$\cdots$	$\cdots$
	Closest distance	4 m	NIST-like	$\cdots$

$$\chi^2 = \sum_{i,j} \frac{[M_{ij} - (\alpha + \alpha_e^i + \alpha_r^j)T_{ij} - (1 + \alpha_b)B_{ij}]^2}{T_{ij} + B_{ij} + (\sigma_{b2b}B_{ij})^2}$$

$$+ \frac{\alpha^2}{\sigma^2} + \sum_j \left(\frac{\alpha_r^j}{\sigma_r}\right)^2 + \sum_i \left(\frac{\alpha_e^i}{\sigma_e^i}\right)^2 + \frac{\alpha_b^2}{\sigma_b^2}. \qquad (3)$$

The χ^2 sums over 14 prompt energy and 15 position bins in the range of [2.0,7.6] MeV and [4.0, 7.0] m, with bin widths of 0.4 MeV and 0.2 m, respectively. The bin widths are comparable to their respective modeled detector resolutions ($10\%/\sqrt{E}$, 0.15 m). Events smeared outside the detector volume are included in the nearest in-detector bin. The sum is minimized with respect to θ_{ee}, Δm_{41}^2 and to the nuisance parameters $\{\alpha, \alpha_r^j, \alpha_e^i, \alpha_b\}$, as described in Ref. [45]. The parameter α allows the signal normalization to vary within the bounds of its associated uncertainty σ to account for uncertainties in the absolute reactor $\bar{\nu}_e$ normalization and absolute detection efficiency. The 100% error in σ ensures a floating overall normalization. This choice of floating overall normalization is made to exclude from the calculated sensitivities contributions from absolute rate deficits, which form the basis of the current ambiguous reactor anomaly signature.

The parameters α_e^i account for the uncertainty in the reactor $\bar{\nu}_e$ spectrum from reactor flux predictions and from previous experimental measurements, as well as detector systematics that are not correlated between energy bins. These parameters allow position bins at one energy to fluctuate together, independently of position bins at any other energy. These fluctuations, correlated in position but uncorrelated in energy, are limited by σ_e^i, which vary as a function of energy as described in Ref. [4]. The energy-uncorrelated σ_e^i are mainly determined by the statistical uncertainty of previous measurements of fission fraction beta spectra. Energy-correlated contributions to the energy spectrum uncertainties also described in this paper are not

included in the σ_e^i. Modeling of these uncorrelated errors in energy is of particular importance, as they limit the power of a pure energy-based oscillation analysis. This will be discussed further in Sec. VIII B.

The position spectrum parameters α_r^j allow correlated fluctuations with position, rather than energy, in order to incorporate the effects of relative efficiency differences and uncertainties between position bins. In contrast to the energy spectrum uncertainties, relative efficiency uncertainties between position bins, given a value $\sigma_r = 0.5\%$ for all bins, should be smaller, as they are easier to characterize via detector simulation and calibration.

Backgrounds B_{ij} are estimated with flat position dependence and a two-component energy spectrum. The first component falls with energy as $1/E^2$, generally mirroring the contribution of low-energy accidental coincidences reported by previous short-baseline experiments [27,31,34,42]. The second component, of equal integrated magnitude in the energy range of the analysis, is flat and extends to higher energy, reflecting the energy signature of fast reactor and cosmic-induced neutrons of widely varying energy. Further detail about the high-energy background shape, such as the exact energy spectrum of proton recoils from fast neutrons, or possible peaks from reactor-induced high-energy gammas, will be highly site dependent. For this reason, these details are not included in the nominal background description. The normalization of this two-component background is allowed to fluctuate similarly to the signal normalization by incorporating the background nuisance parameter α_b, with an associated systematic uncertainty of $\sigma_b = 10\%$.

In order to resolve spectral distortions in the energy and position distribution of signal events, it will be necessary to characterize the uncorrelated uncertainties in the background energy and position spectrum. Background position and energy spectrum uncertainties are not likely to be decoupled, as is the case for the signal position and energy
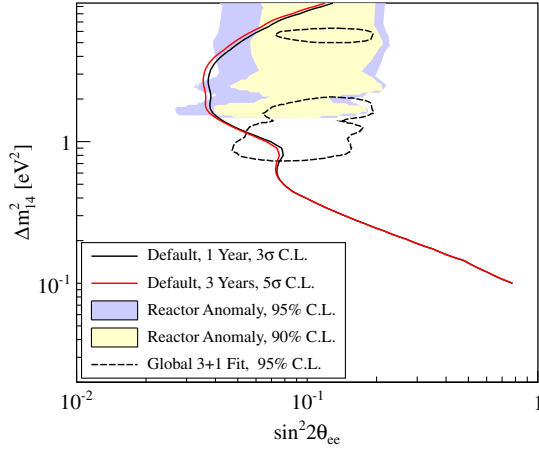
FIG. 3 (color online). Sterile neutrino oscillation discovery potential at 3σ and 5σ for the nominal experimental arrangement described in Table I. The 3σ contour corresponds to one year of detector live time while the 5σ contour is shown for three years of detector live time. Also pictured are the best-fit parameter spaces for the reactor antineutrino anomaly [6] and for the $3 + 1$ global fit to all relevant accelerator, source, and reactor data given in Ref. [7].

spectrum uncertainties. For example, the signal energy spectrum in the absence of oscillations is the same for every position bin, while the background energy spectrum may vary in normalization and shape from position to position, depending on many variables, such as variations in fast neutron fluxes or effective passive shielding with position. Without the specifics of these correlations, the most conservative way to incorporate these background uncertainties into the χ^2 analysis is to provide an additional independent nuisance parameter for every bin with an associated uncertainty σ_{b2b} that reflects the precision of any background spectral measurements. Conservative consideration of these uncertainties can be more simply achieved by adding the

effect of σ_{b2b} to the denominator of the χ^2. For this study, σ_{b2b} is given a default value of 0.5%.

It should also be noted that no assumptions about specific background subtraction or reduction techniques are included in these sensitivity calculations. The background shape and uncertainties are included in the χ^2 as described above, and the derived sensitivities represent the experiment's scientific reach under the stated assumptions. Future R&D efforts will study the distribution and magnitude of site-specific backgrounds and develop techniques to mitigate and reduce their impact on a VSBL experiment.

For the nominal experimental arrangement described in Table I as well as for the varied cases to follow, 3σ and 5σ discovery potentials for neutrino oscillations are calculated following the prescription in Ref. [45]. Example discovery contours from the nominal experimental setup are shown in Fig. 3. The nominal arrangement considered in Table I is capable of excluding a large fraction of the currently preferred parameter space to better than 3σ with 1 year of live time and at 5σ C.L. with 3 years of data taking. Sections IV, V, and VII, investigate the impact of the reactor, facility, and detector parameters on the sensitivity of the experiment. The experimental parameters listed in Table I will be used throughout this paper as the nominal experimental arrangement.

IV. REACTOR PARAMETERS

A. Reactor power and operations

The flux of $\bar{\nu}_e$ emitted from reactors is directly related to its thermal power. The total nominal power capacities for several research and commercial reactor sites are shown in Fig. 4. At 3 GW$_{th}$, typical commercial power stations such as SONGS [46,47] are about an order of magnitude more powerful than research reactors. Research reactors in the U.S. have a wide range of thermal powers up to a maximum of 250 MW at the Advanced Test Reactor [41]. The
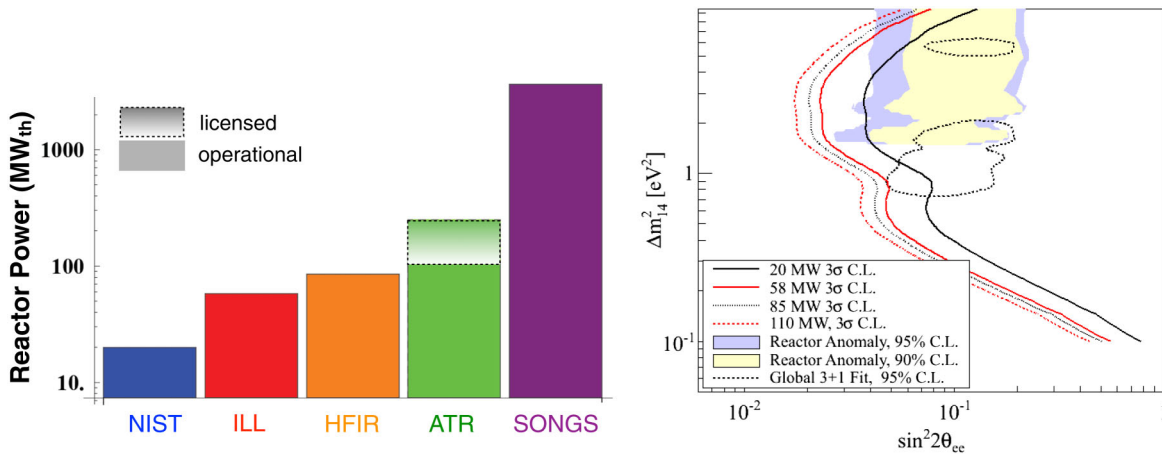

FIG. 4 (color online). Left: Comparison of nominal and operational thermal power output for selected reactor facilities. The nominal licensed power output (dashed line) is roughly equal to the operational power (solid line) for all facilities except the Advanced Test Reactor. Right: Sensitivity of the nominal experimental configuration for various power levels and 1 year of detector live time.

TABLE II. Summary of reactor powers, accessible baselines, fuel cycles, and reactor-off times at various reactor facilities. At ATR, detector access is limited for baselines <12 m. SONGS data are from past operation; this facility is currently shut down. The estimated down-time fraction includes estimates of occasional longer seasonal shutdowns and maintenance periods based on communication with the respective reactor facilities.

Reactor	Power (MW_{th})	Baselines (m)	Reactor on (days)	Reactor off (days)	Down time	Reference
NIST	20	4–20	42	10	~32%	[39]
HFIR	85	6–8	24	18	~50%	[40]
ATR	250 (licensed) 110 (operational)	7–8 (restricted) 12–20 (full access)	48–56	14–21	~27%	[41]
ILL	58	7–9	50	41	~45%	[48]
SONGS	3438	24	639	60	8.6%	[46,47]

variation of the experimental sensitivity of the baseline experimental configuration with the power of several research reactors (or $\bar{\nu}_e$ flux) is shown in Fig. 4. The increase in event statistics with thermal power uniformly increases an experiment's sensitivity for all values of Δm^2.

Nuclear reactors are periodically shut down for refueling and maintenance. As a result, the time-averaged thermal output of a nuclear reactor will be less than its maximum thermal output over that time period because of periods of below-capacity operation and reactor-off periods. For example, at ATR the standard operating thermal output of 110 MW is significantly below its maximum licensed thermal output of 250 MW. See Fig. 4. All nuclear facilities undergo reactor-off periods in which reactor refueling and maintenance takes place. Table II summarizes the length and frequency of reactor-off periods at several reactor facilities as well as their reactor-on and -off time.

Reactor-off time and operation at reduced power directly reduce the total annual $\bar{\nu}_e$ event statistics yielding the same net effect as a lower thermal power capacity. Sensitivity to sterile oscillations decreases with lower power as illustrated in Fig. 4. However, reactor-off time provides an opportunity to measure the rate and energy distribution of backgrounds. A detailed understanding of the spatial and energy distribution of backgrounds is critical for a precision experiment at short distances from the reactor. This topic will be discussed in greater detail in Sec. VI. The optimum ratio of background measurement time relative to $\bar{\nu}_e$ signal time will depend on the total signal statistics, the dominant uncertainties, as well as the signal-to-background ratio. This optimization should be carried out as part of a detailed design process for a VSBL experiment. For the research reactors in Table II the $\bar{\nu}_e$ signal time will be between 50% and 73% of calendar time.

B. Reactor fuel

Commercial nuclear power stations use conventional nuclear fuel comprised of a mixture of U and Pu isotopes while some research facilities operate with HEU. The decay chains of the four isotopes ^{235}U, ^{238}U, ^{239}Pu, and ^{241}Pu produce >99.9% of all $\bar{\nu}_e$ produced in a reactor. In HEU cores nearly all fissions are accounted for by ^{235}U.

Table III gives the main fission isotopes in the two reactor fuels and their relative contributions to the total fission rate.

The $\bar{\nu}_e$ spectrum and rate per fission is different for each of these isotopes [50] and the flux and spectrum of reactor $\bar{\nu}_e$ are the sum for all isotopes in the reactor core. The time-averaged detected $\bar{\nu}_e$ spectra from HEU and conventional fuels are compared in Fig. 5. The integrated flux differs by roughly 8%, and the time-averaged spectral differences are 10% or less. In addition, the time evolution of the isotopic fuel composition creates a time-dependent spectral shape. For the spectral range shown in Fig. 5 the typical fission fractions for the average fuel were evaluated and compared to the upper and lower fractions at the beginning and end of fuel cycle [24]. Using the spectral shapes from Ref. [50] together with the isotope fraction, the combined spectrum can be calculated. When convoluted with the standard inverse beta cross section, we obtain the detected $\bar{\nu}_e$ spectrum. The differences in the energy spectrum only have a small impact on sensitivity to short-baseline neutrino oscillation as shown in Fig. 6.

In addition to differences in the integrated flux and spectral shape, the uncertainties spectral shape vary between the dominate fission isotopes. These arise from a combination of the statistical and measurement uncertainties of fission isotope beta spectra [31] and uncertainties in the conversion of electron spectra to corresponding $\bar{\nu}_e$ spectra [4,51,52]. Spectral uncertainties for ^{235}U range from 1.8% to 3.2% in the range from 2 to 6 MeV, while for ^{239}Pu they increase to 1.9%–5.7% and 2.5%–5.0% for ^{241}Pu [53]. Because of these considerations, spectral uncertainties will be lower for HEU

TABLE III. Approximate time-averaged fuel compositions for various reactor cores. Fractions for conventional [24] and HEU reactors [49], respectively.

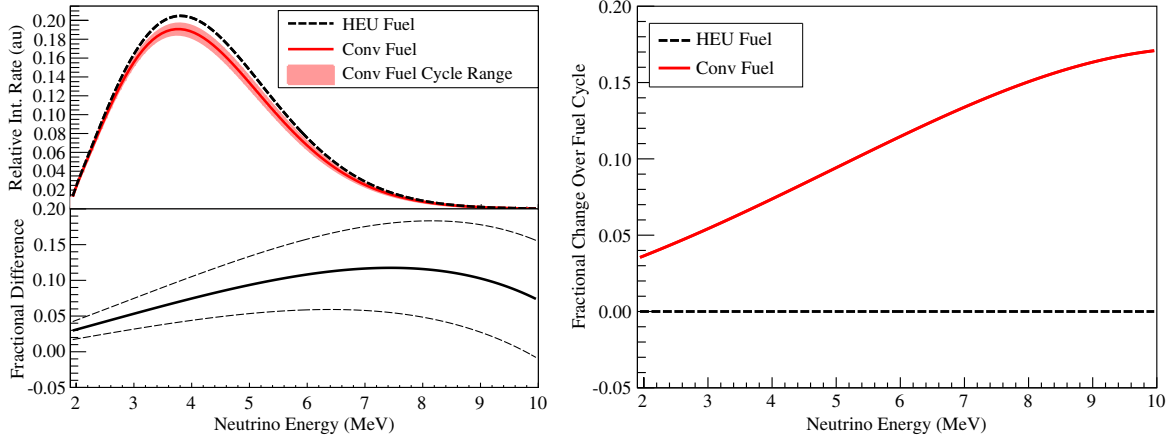| Fuel isotope	Time-averaged fission fraction	
	Conventional fuel	HEU fuel
^{235}U	0.59	>0.99
^{238}U	0.07	<0.01
^{239}Pu	0.29	<0.01
^{241}Pu	0.05	<0.01

FIG. 5 (color online). Left: Detected reactor $\bar{\nu}_e$ spectra from conventional commercial and HEU fuel (top panel), and their spectral differences (bottom panel). The band indicates the change in the spectral shape over one fuel cycle. Right: Fractional change in spectrum over one fuel cycle for conventional and HEU reactors.
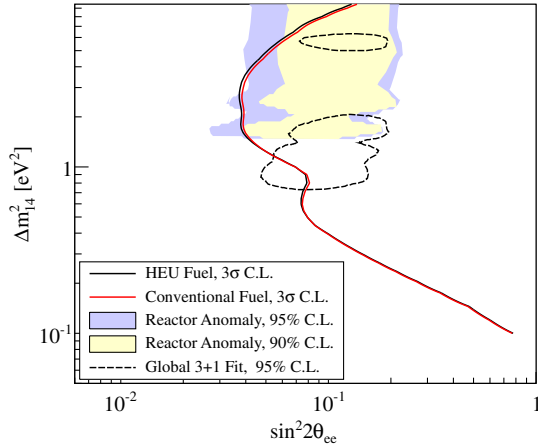

FIG. 6 (color online). Sensitivities of the nominal reactor experiment for conventional and HEU fuel reactor cores. The use of HEU fuel leads to minor improvements in the overall sensitivity.

fuel than for conventional fuel. The change in sensitivity resulting from this difference in spectral uncertainty for the two fuel types is shown in Fig. 6. HEU fuel provides a minor improvement in sensitivity as a result of the lowered spectral uncertainties. The benefits of lower spectral uncertainties will be amplified in the case of detectors with limited baseline ranges or position resolution, as will be discussed in Sec. VIII B.

C. Reactor core size and dimensions

Reactor cores come in a wide variety of shapes and sizes. The $\bar{\nu}_e$ production in a reactor follows closely the distribution of the fuel assemblies. For the purpose of a neutrino oscillation experiment at very short baselines the main difference between commercial power reactors and research reactors is in their size. Conventional pressurized water power reactors are typically 3–4 m in height and

diameter, while research reactors tend to be smaller in size with dimensions as compact as ~0.5 m or less. Figure 7 provides an illustration of the variety of shapes and sizes of various research and conventional reactor cores.

For neutrino oscillation searches it is required that the size of the reactor core and thus the spread in neutrino path lengths to be less than the oscillation wavelength to avoid a washout of the oscillation signal. Figure 7 shows the spread in path lengths between the finite-sized reactor cores and a pointlike detector horizontally displaced from the vertical midpoint of each reactor at a distance of $r = 10$ m. The distance r is defined between the geometric center of the core and the pointlike detector. A distance of $\mathcal{O}(10\text{ m})$ represents a typical distance for a very-short-baseline reactor experiment. We assume that neutrinos are produced and emitted uniformly throughout the core region. We define the path length l as the distance between the points of $\bar{\nu}_e$ production and observation. Convolving the path length distribution with $1/R^2$ determines the expected spatial distribution for the relative probability of $\bar{\nu}_e$ interactions in the detector. We note that a detector with finite position resolution or segmentation adds additional smearing to the observed path length distribution and the observed oscillation effect.

For finite-sized reactor cores of any geometry we can calculate the average path length $\bar{l}$ and the rms of the path lengths as

$$\bar{l} = \frac{1}{\text{volume}} \int_{\text{vol}} \sqrt{x^2 + y^2 + z^2}\, dx\, dy\, dz \quad \text{and} \quad (4)$$

$$l_{\text{rms}} = \sqrt{\frac{1}{\text{volume}} \int_{\text{vol}} \sqrt{x^2 + y^2 + z^2 - \bar{l}^2}\, dx\, dy\, dz}. \quad (5)$$

Figure 8 shows the average neutrino path length spread for different core geometries as a function of distance from the reactor. At $d > 5$ m the rms spread in path lengths
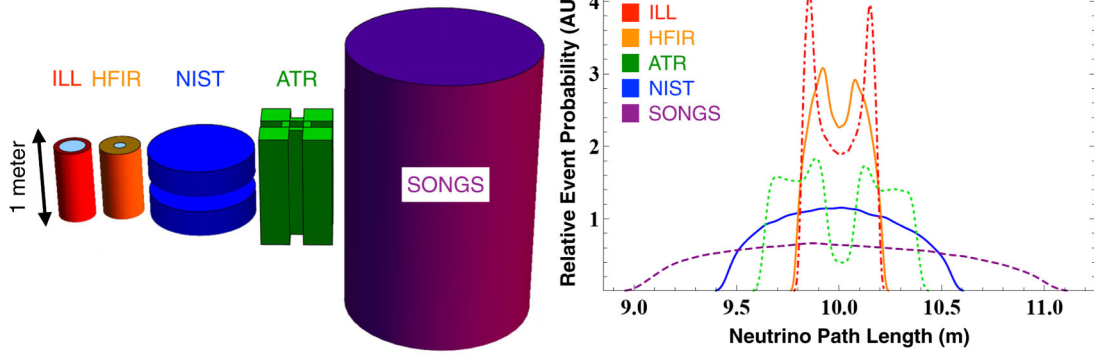
FIG. 7 (color online).   Left: Approximate size and shape of fuel distribution in five reactors including the U.S. research reactors ATR, NIST, and HFIR. SONGS is a conventional power reactor, for comparison. Right: Relative event probability versus neutrino path lengths for several finite-sized reactor cores and a pointlike detector horizontally displaced from the vertical midpoint of each reactor at a distance of $r = 10$ m.
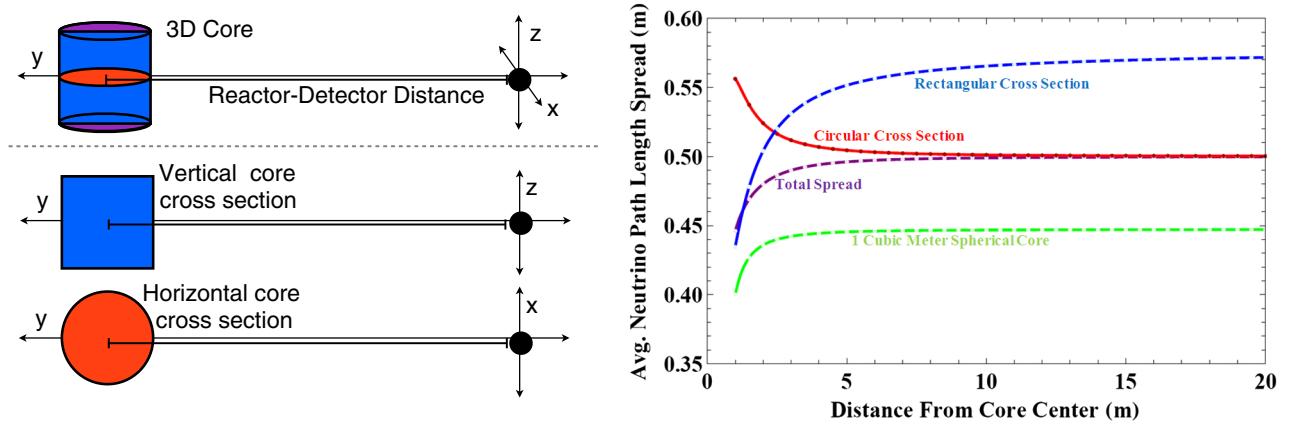

FIG. 8 (color online).   Left: Geometries, cross sections, and path lengths for a cylindrical reactor core and pointlike detector. Right: Corresponding path length spreads for a 1-m cylindrical core. The differences in path length spreads contributed by the circular horizontal dimensions and the rectangular vertical dimensions of the core are a small correction on top of the overall magnitude of the spread, which is defined by the overall core size.
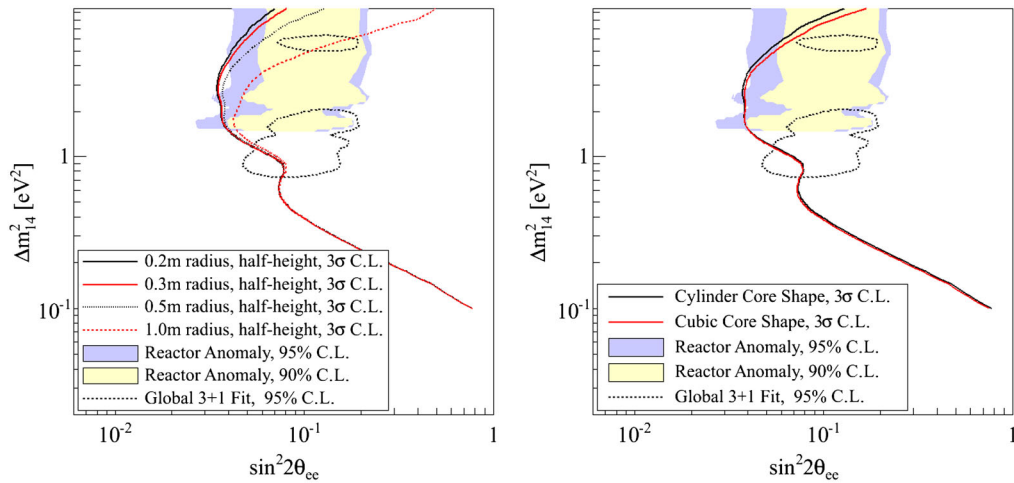

FIG. 9 (color online).   Variations in the discovery potential of the nominal reactor experiment with a half-height core of various radii (left) and core geometries (right). The overall spread in neutrino path lengths is dominated by the overall dimensions of the core.

approaches ∼0.5–0.6 m for a reactor of 1 m height and diameter. The variation due to the core shape is significantly smaller than the total magnitude of spread. For all practical considerations and for realistic distances of $d > 4$ m from the reactor the shape of the core and fuel distribution is only of secondary consideration. For highly asymmetric cores such as long, cylindrical arrangements choosing the orientation of the detector with respect to the symmetry axis of the core can be used to reduce the spread in neutrino path lengths. Figure 9 shows the discovery potential of the nominal reactor experiment for varying dimensions of the reactor core. The sensitivity to higher Δm^2 values is lost as the core width is increased. The overall core dimensions dominate the spread in neutrino path lengths while the core shape only plays a secondary role.

V. FACILITY PARAMETERS

A. Experimental area and detector volume

A key signature of neutrino oscillation is the distortion of the measured spectrum with energy and the variation of the energy spectrum with baseline. The baseline dependence of the energy spectrum can only be observed in a detector whose active length comprises more than a small portion of one oscillation period. Ideally, one would map out the oscillation over an entire wavelength or more. The availability of experimental space in a reactor facility limits the accessible baselines as well as the total active detector volume. The accessible baselines listed in Table II provide a distance range of up to 9 m at one particular facility. This allows the placement of several small detectors in various locations, or the construction of an extended detector in the radial direction. For any significantly extended detector the change in event rate due to the $1/R^2$ law has to be taken into account.

An increase in detector length has two effects: It increases the total overall event statistics of the experiment and it samples a larger fraction of the possible oscillation wavelength. Both the maximum achievable sensitivity and the overall range of accessible Δm^2 values improve with an increase in detector length. In particular, sensitivity to lower values of Δm^2 is improved with a longer detector as oscillations with longer wavelength are sampled. Figure 10 shows the change in sensitivity of an experiment with the default characteristics for three different detectors of 1, 3, and 5 m lengths. Figure 10 shows on one side the overall sensitivity of the three detectors with the different event statistics due the various detector lengths and on the other hand the same experimental arrangement normalized to the statistics of the default experiment. The normalized case illustrates the impact of the detector length or baselines while the un-normalized situation highlights the decrease in event rate with $1/R^2$.

The detector cross section is typically limited by space constraints inside the containment building near the reactor core. As the overall target mass and thus statistics at each baseline scale with the cross-sectional area of the detector, one can consider scaling the cross-sectional area of the detector as a function of baseline to counteract the effect of the $1/R^2$ reduction in flux.

B. Reactor-detector distance

For extended core and detector geometries, the distance between the reactor and the detector is not uniquely defined. We therefore choose the reactor-to-detector distance r as the distance between the center of the reactor core and the closest point to the reactor in the active detector region while the detector length d describes the radial length of the active detector volume. The reactor-to-detector
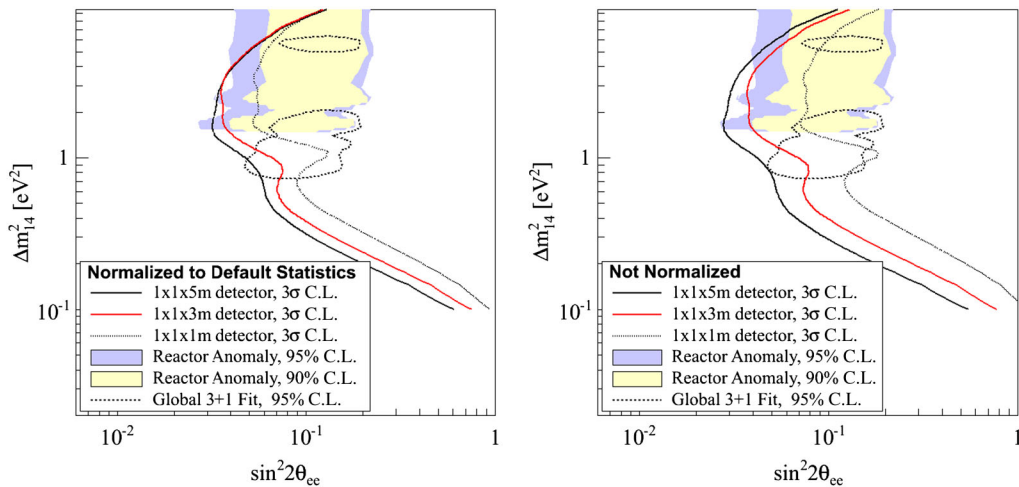

FIG. 10 (color online).   Variation in sensitivity of the default experiment with detector length. Left: Event statistics is normalized to the default experiment in each case. Both the maximum achievable sensitivity and the range of accessible Δm^2 are increased with increased detector length. Right: Un-normalized case demonstrates the additional effect of increased statistics with larger detector volume.
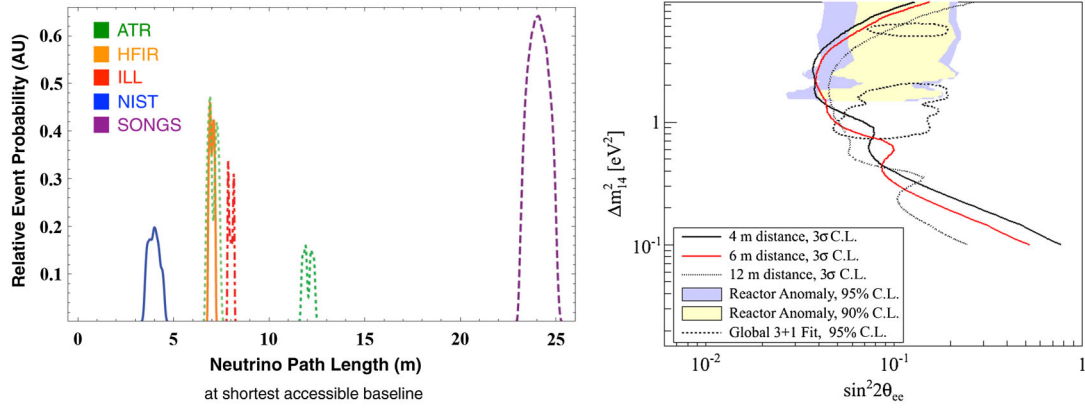
FIG. 11 (color online).   Left: Relative probability of $\bar{\nu}_e$ interactions in a pointlike detector at the closest possible distance from the respective reactor cores. The spread in neutrino path lengths reflects the size and shape of the reactor cores. The peak areas give the relative reactor power scaled by $1/R^2$. Right: Sensitivity of the default configuration for closest accessible baselines of 4, 6, and 12 m, respectively. To emphasize only the effect of baseline, the normalization is adjusted to provide equal total event statistics.

distance r, at a minimum, is comprised of the extent of the reactor itself and the thickness of the containment and shielding structures surrounding the core. In practice some passive shielding will be required to operate a $\bar{\nu}_e$ detector in the vicinity of a reactor. The accessible baselines for various reactor facilities listed in Table II take 0.5 m additional space into consideration for this purpose. The closest accessible baseline is site specific and referred to as $r_{\min}$. As is shown in Table II, research reactors provide an opportunity for improved measurements of the reactor $\bar{\nu}_e$ flux and spectrum at the shortest baselines to date. Facilities such as NIST may provide access to baselines as short as 4 m or less.

In maximizing event statistics and experimental sensitivity, the design of an experiment is a trade-off between distance, spread in neutrino path length, and relative reactor power. Figure 11 shows the spread in neutrino path lengths from finite-sized reactor cores as seen by a pointlike detector at the closest accessible baseline $r_{\min}$. The spread in neutrino path lengths reflects the size of the reactor cores while the area of each distribution indicates the relative reactor power scaled by $1/R^2$.

The right panel of Fig. 11 shows the sensitivity of the default experiment for $r_{\min} = 4$, 6, and 12 m, respectively. To emphasize the effect of varying $r_{\min}$, the normalization is adjusted to maintain the same total statistical sensitivity in each case. The closest accessible baseline, $r_{\min}$, impacts the high-Δm^2 sensitivity of the experiment. This is due to the fact that finite energy resolution tends to wash out the observed oscillation with distance from the reactor core.

The effect of $r_{\min}$ on sensitivity to oscillation at various ranges of Δm^2 is dependent on the total detector length d. Longer detectors help improve the sensitivity to lower values of Δm^2 but do not compensate completely in case of larger $r_{\min}$. This is illustrated in Fig. 12 for a 3 m-long detector placed at 4 and 12 m, respectively, from the reactor core. Figure 12 illustrates how a detector of chosen

length samples different fractions of the oscillation periods and oscillation amplitudes for various Δm^2. For larger Δm^2, the best achievable sensitivity at large $r_{\min}$ is lower even with longer detectors because the amplitude of the oscillation is diminished. For low Δm^2, only a small portion of the oscillation period fits inside the detector length at both distances, indicating the need to sample a much
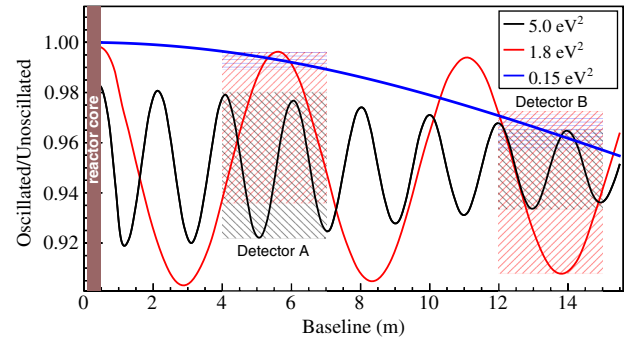

FIG. 12 (color online).   Oscillation of 4 MeV $\bar{\nu}_e$ for Δm^2 of 6.0, 1.8, and 0.15 eV^2 as a function of baseline. The shaded regions indicate the position and radial dimension of the detectors for the default experimental configuration. The dimensions of the reactor core are shown in solid color. Oscillation curves include position smearing resulting from position resolution and from the finite reactor core size. Boxed areas indicate the range of oscillated/unoscillated oscillation amplitudes covered by each case. For the large Δm^2 value (5 eV^2), the 3 m detector length encapsulates more than a full period, and the damping of the oscillation amplitude due to finite detector resolution reduces the visible oscillation at farther distances. For medium Δm^2 values (1.8 eV^2), the 3 m detector length allows for significant observation of oscillation at both distances. For very small Δm^2 (0.15 eV^2), the variation in oscillation from detector front to back is larger at 12 m than at 4 m, although both differences are small, as the 3 m detector length encapsulates only a small portion of the total period. Two detectors at different baselines may be needed to probe regions of small Δm^2.

longer range of baselines. For the favored mass splitting the oscillation period is sampled well at both chosen baselines.

If the oscillation length were known *a priori*, a detector of suitable length could be placed between the first oscillation minimum and subsequent maximum to maximize the observed oscillation difference or around the oscillation minimum to observe the turning point. Ideally, such a detector would be movable to measure both the difference between the oscillation maximum and minimum and the turning point around one of the oscillation extreme. A movable, extended detector can also help mitigate possible backgrounds or systematic effects that can mimic this oscillatory signature. In the case of longer wavelengths and given the facility constraints at research reactors, multiple, radially extended detectors may be necessary to allow for a comprehensive search for and discovery of neutrino oscillations with unknown Δm^2.

VI. BACKGROUNDS

The overall magnitude and spectral shape of backgrounds in a short-baseline reactor neutrino experiment are determined in large part by the detector's surroundings, including overburden, the distance to the core, neutron backgrounds from the reactor and nearby experiments, cosmic ray induced backgrounds, and nearby spent fuel repositories. The cleanliness of the detector components determines the magnitude of low-energy backgrounds.

The contribution of each of the various background types can be significantly reduced by implementing a wide array of background reduction techniques. The use of passive shielding can reduce the number of gamma and neutron backgrounds incident on the detector target by orders of magnitude. Detector optical segmentation affords the ability to distinguish signal events based on their spatial distribution, which will be significantly different than that

of many types of backgrounds, particularly accidentals [31,36,54,55]. The use of scintillator with pulse-shape discrimination abilities will also increase the ability to distinguish the prompt positron of an inverse beta interaction with the prompt proton recoil of a fast neutron interaction. The use of doped liquid scintillators using Li or Gd can also reduce inverse beta time coincidence, leading to higher muon veto efficiencies and lower accidental background rates. Suitable pulse-shape discrimination and doped liquid scintillators have been utilized in previous experiments (for example, Ref. [36]) and are a subject of significant current R&D efforts [26,56–59].

Clearly, the exact shape and magnitude of backgrounds and signal efficiency from background reduction cuts in a prospective VSBL experiment vary widely and can be precisely known only by conducting site-specific background surveys, detector material surveys, and detector design and simulation studies. This paper seeks to provide guidance to this R&D process by varying key background metrics to determine the necessary background reduction requirements of a sufficiently sensitive VSBL sterile oscillation experiment.

To determine the background rates necessary for a highly sensitive VSBL oscillation experiment, the sensitivity of the default experiment to varying background conditions was investigated by varying the magnitude and shape of the input background spectrum in the χ^2 calculation. Signal-to-background ratios of 0.1, 1.0, and 10 were considered. Changes in sensitivity resulting from variation of S/B ratio of the default experiment can be seen in Fig. 13. The overall background rate clearly has a significant impact on experimental sensitivity at all values of Δm^2. If sensitivity to the full range of suggested sterile oscillation parameter space is desired, S/B ratios of 1 or better are likely necessary.

In order to achieve these signal-to-background goals, particularly in the case of high accidental backgrounds, it
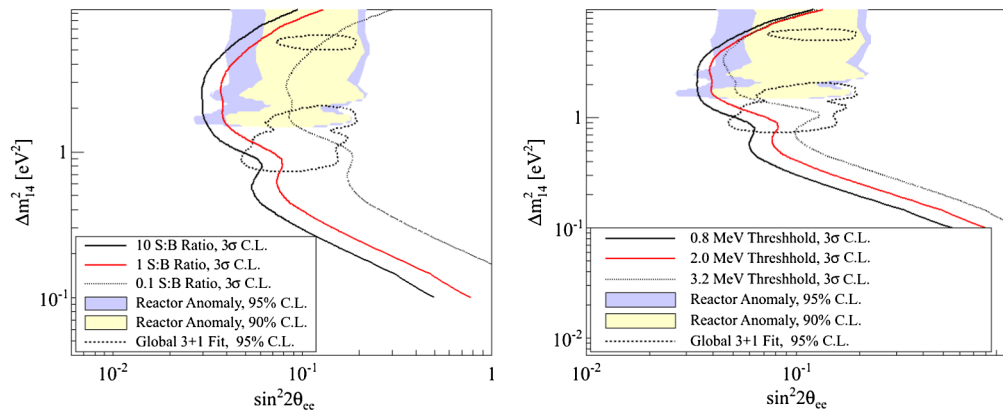

FIG. 13 (color online). Variation in sensitivity of the default experiment with overall signal-to-background (left), low-energy threshold (right) and spectral shape (bottom). The default parameters used throughout the paper are a S/B ratio of 1:1 with a 2.0 MeV energy threshold and a $1/E^2$ + flat spectral shape. Backgrounds will clearly play a critical role in the experimental sensitivity at a broad range of Δm^2 values.

may be necessary to adjust the prompt energy cut threshold. Figure 13 also shows sensitivity for the default arrangement assuming a S/B of 1 for various prompt energy cut thresholds from 0.8 to 3.2 MeV. The higher threshold clearly excludes the low-energy portion of signal events, leading to lower sensitivity particularly at lower δm^2 values.

As defined in the χ^2 given in Eq. (3), backgrounds are assigned a nuisance parameter that accounts for the uncertainty in the overall background normalization. Wide variation of this parameter's associated systematic uncertainty has negligible effect on the sensitivity of the default experiment.

Background spectral shapes were also varied in addition to overall background normalization. Three different background spectral shapes, pictured in Fig. 14, were used: the default $1/E^2$ shape seen in previous short-baseline experiments [27,31,34], a flat distribution commonly associated

in deep-underground reactor $\bar{\nu}_e$ experiments with fast neutron backgrounds, and a distribution identical to the signal distribution. The results of these variations are also shown in Fig. 13. The overall background normalization appears to have a much larger effect on sensitivity than the exact spectral shape within the assumptions of this study. The same is also found to be true for the shape of the background position distribution.

As discussed in Sec. III C, uncertainties in the background energy and position spectrum shapes, without site-specific background surveys, conservatively accounted for with the addition of σ_{b2b} to the denominator of the χ^2. To determine the effect of this uncorrelated spectral uncertainty on overall sensitivity, σ_{b2b} was varied for the default experiment from 0.5% to 10.0%. The effect of this parameter is illustrated in Fig. 14: each bin in energy and position is effectively allowed a free, uncorrelated fluctuation within a band determined by σ_{b2b}. For a real
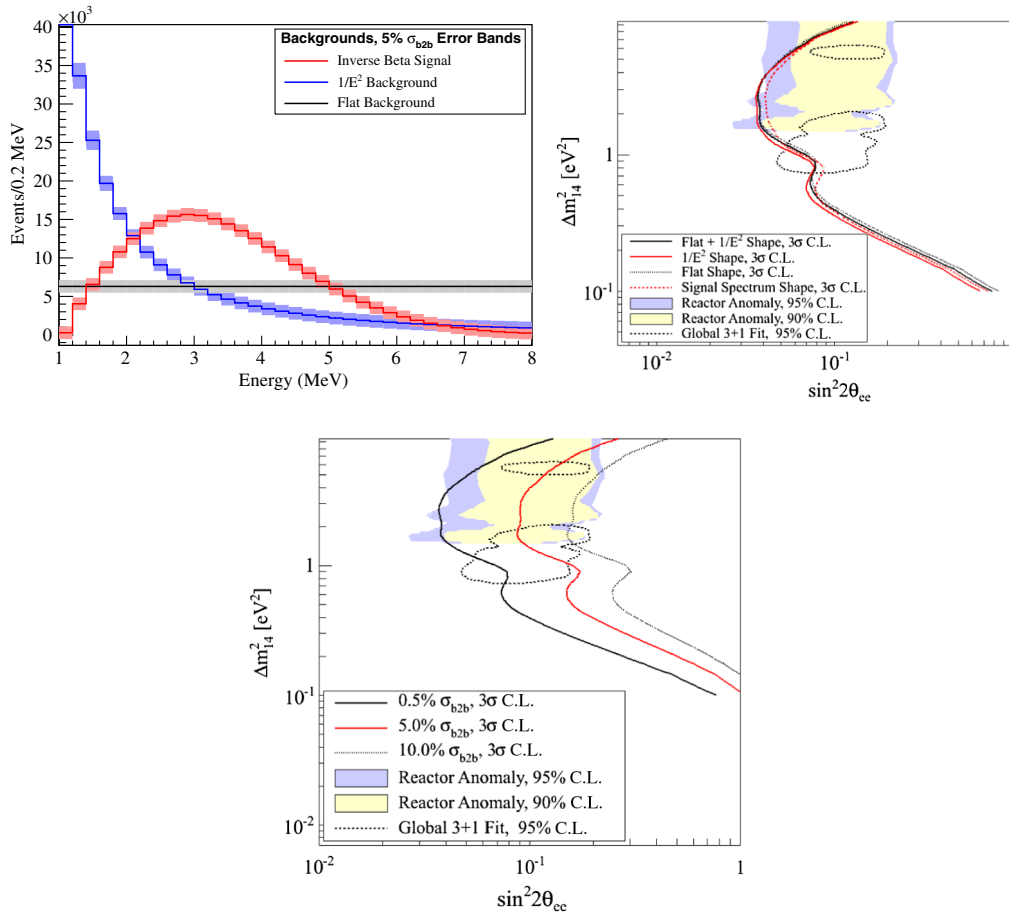

FIG. 14 (color online). Left: Example signal and background energy spectra. The $1/E^2$ background represents the spectral shape provided by accidental backgrounds mainly from intrinsic detector radioactivity, while the flat background provides a crude model of the energy spectrum from fast neutrons. The default signal:background ratio is 1, with a spectral shape split evenly between the flat and $1/E^2$ distributions. A 5% uncertainty band is indicated on each spectrum for reference. Right: Minor variations in sensitivity for various background shapes. Bottom: Sensitivity of the default experiment to sterile neutrino oscillations for various values of σ_{b2b}. The significant variation in sensitivity with σ_{b2b} underscores the importance of a precise knowledge of the background energy and position spectrum.

experiment, the magnitude of σ_{b2b} will be determined by measurements of background spectra during reactor-off periods, as well as measurements of low- and high-energy singles during reactor-on periods. Shifting the detector radially may also help map out and constrain the spatial variation of the backgrounds. The resultant change in sensitivity of the default experiment with variations in σ_{b2b} are also shown in Fig. 14. Sensitivity to oscillation is highly dependent on σ_{b2b} for all values of Δm^2. Precise knowledge of the background spectral shapes is clearly necessary for a definitive short-baseline oscillation experiment.

VII. DETECTOR PARAMETERS

A. Target mass and efficiency

The total neutrino interaction rate scales proportionally with target mass and detection efficiency. Variations of target mass and efficiency have an identical effect on the sensitivity as variations in reactor power. Thus, the effect of variations in efficiency can be interpreted from Fig. 4. The target mass can be increased by increasing the cross section of the detector, which is largely constrained by the available facility space, or by increasing the proton density of the target.

The main contributors to lowered detection efficiency can be addressed with the application of appropriate detection techniques:

(i) *Muon and singles dead times.*—Muon veto efficiency is determined by the total detector muon flux (200–500 Hz for various on- or near-surface LS experiments [32,55]) and by the width of the vetoed time window after a muon. Doped scintillators can maintain inverse beta coincidence times of less than 50 μs [16,26,58]. Combination of the surface muon flux with a short veto window should allow for reasonable muon veto efficiencies. Shorter coincidence times also should reduce the

number of signal events that are rejected because they are accompanied by an unrelated detector trigger.

(ii) *Delayed signal efficiency.*—Delayed signal efficiencies can be improved over previous experiments if necessary by reducing the delayed signal's spatial spread through techniques such as Li doping.

(iii) *Prompt signal efficiency.*—Prompt signal efficiencies can be improved over previous experiments if necessary by lowering the low-energy analysis threshold if possible, or by increasing the pulse shape discrimination power, if used in the analysis.

B. Detector resolution and analysis binning

Independent of a specific reactor-detector orientation and facility space constraints, the detector parameters that define the sensitivity of an experiment are the detector's energy and position resolution. Good energy resolution is needed to both resolve the spectral distortions at a particular baseline and avoid washing out the oscillation at longer baselines, while position resolution allows for the observation of an oscillation as a function of distance. Previous short-baseline experiments have demonstrated the ability to attain sub-10% energy resolution [36,38], while larger θ_{13} liquid scintillator detectors have achieved resolutions of around 7%–8% [44]. Acceptable position resolution can be obtained either through optical segmentation of the detector volume, or by using charge topology information to reconstruct event positions in a larger one-zone detector. The former technique has been demonstrated in a number of previous short-baseline experiments, such as Palo Verde and Bugey [36,54], while the larger gadolinium-loaded liquid scintillation detectors at Daya Bay, RENO, and Double Chooz have demonstrated successful position reconstruction with a resolution of 30 cm or better [17,34].

Figure 15 demonstrates the effect of variations in detector resolution for the default experiment. The fractional
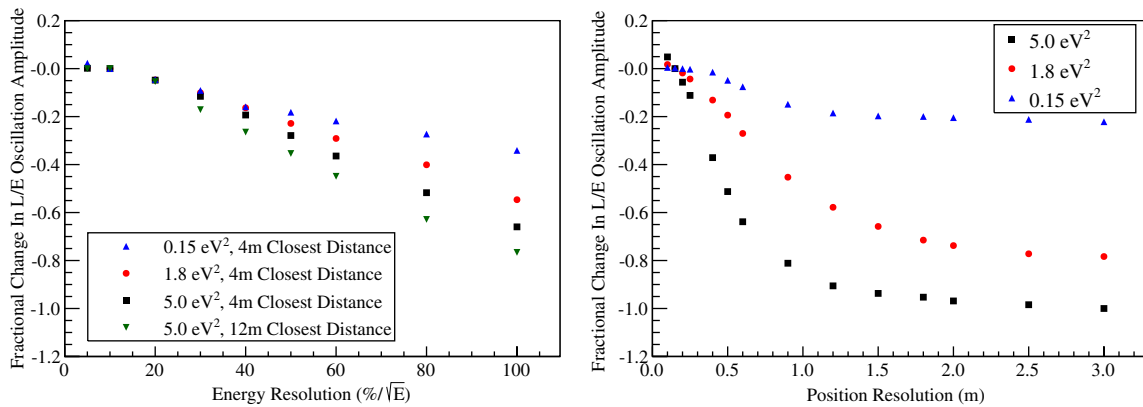

FIG. 15 (color online). Fractional change in detected oscillation amplitude with changes in energy (left) and position (right) resolution for the default experiment at either 4 or 12 m closest distance. Δm^2 values of 0.15, 1.8, or 5.0 eV^2 are used. Fixed values of 10% for energy and 15 cm for position are used when varying position resolution and energy resolution, respectively.
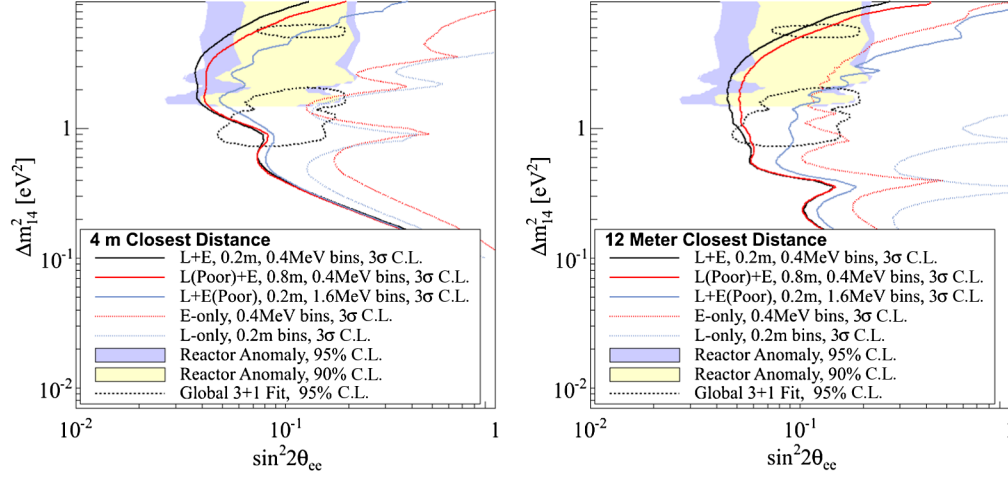
FIG. 16 (color online). Variation in sensitivity to short-baseline oscillations with energy and position bin size for the default experiment at closest distances of 4 (left) and 12 m (right). Statistics are normalized to the level of the default experiment, 220 000 $\bar{\nu}_e$/year. Sensitivity is degraded, particularly at high Δm^2, as bin width is increased. One can also see the differing contributions to the total sensitivity from position and energy information, and how this contribution changes with differing detector closest distance.

change in amplitude of the measured L/E oscillation pictured in Fig. 2 is taken as the figure of merit. The oscillation signature is increasingly washed out as the position and energy resolution decrease. Attaining an energy resolution of better than 10% will not provide significant gains in sensitivity for this range of Δm^2. Position resolution in the vicinity of 20–30 cm will be necessary to detect 90% or better of the optimal oscillation amplitude.

The effect of finite position and energy resolution can be approximated by varying the bin width in the χ^2 analysis: the bin width provides an effective limit on the knowledge of exact event baselines and energies. The results of this approach are pictured in Fig. 16. The average $\bar{\nu}_e$ detections in each bin are given in Table IV to give a sense of the statistics provided by each binning. It is clear that sensitivity to high Δm^2 values is degraded as bin width is increased.

Figure 16 also illustrates qualitatively the individual contributions of energy and position information to the total sensitivity. As the binning in energy or position, and thus the information available from energy or position, is reduced, sensitivity is reduced evenly, indicating that the two variables contribute roughly equally to the overall

sensitivity of the default experiment. This is a feature of our choice of a default detector and the resolutions considered. Figure 16 also presents sensitivity for various binning choices of the same arrangement at 12 m closest distance. For this arrangement, sensitivity is reduced much more quickly when energy binning is reduced, indicating that energy information provides most of the experimental sensitivity and that energy resolution is of paramount importance for longer-baseline detectors.

VIII. SUMMARY AND DISCUSSION

A. Key experimental parameters for an experiment at very short baselines

In this paper we have studied the optimization of a very-short-baseline oscillation experiment utilizing an HEU core with the highest possible power and smallest core size. To probe eV-scale mass-squared splittings, we consider a detector of at least 3 m at the shortest possible core distance with the highest possible efficiency, energy resolution of better than 10%, and position resolution of better than 0.2 m. Furthermore, a S/B ratio of at least 1:1 at low analysis threshold is desirable. The experiment may benefit

TABLE IV. Number of events per bin versus analysis binning for the default experiment with 1 year of live time. 220 000 total $\bar{\nu}_e$ detections are expected with the default experiment.

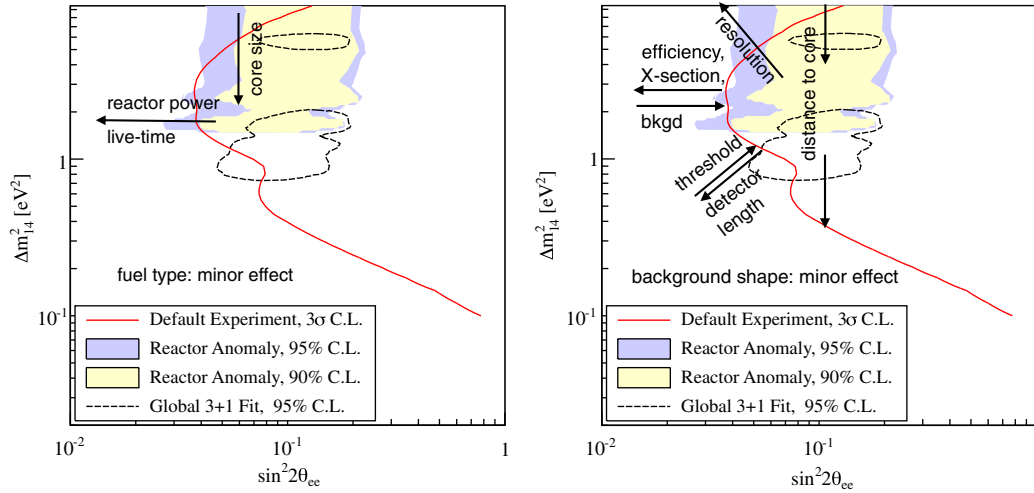| Number of bins			
Energy	Position	Events per bin	Comment
14	15	1050	Energy + position analysis, (0.4 MeV, 0.2 m) binning
14	4	3900	Energy + position(poor) analysis, (0.4 MeV, 0.8 m) binning
4	15	3700	Energy(poor) + position analysis, (1.6 MeV, 0.2 m) binning
1	15	14 700	Position-only analysis, 0.2 m binning
14	1	15 700	Energy-only analysis, 0.4 MeV binning

FIG. 17 (color online).   Reactor and detector parameters relevant for covering the suggested parameter space. The arrows indicate the direction in which the sensitivity curve moved when reactor (left) and detector (right) parameters are improved or adjusted.

from a second or third detector at longer baselines of 10–20 m to improve sensitivity to the regions of small Δm^2.

Figure 17 qualitatively summarizes the impact of various reactor and detector parameters on the parameter space covered by very-short-baseline reactor $\bar{\nu}_e$ experiments. The relative importance of these parameters is not weighted in this figure, and some experimental variables such as the precise core shape have only secondary effects on the experiment.

(i) *Total statistics.*—The per-bin statistical uncertainty can be a limiting quantity when searching for oscillations over numerous energy and position bins. By utilizing a core with the highest possible power and a detector with the highest possible efficiency, cross section, or proton density, one can maximize this quantity and considerably improve an experiment's sensitivity to short-baseline oscillations at all Δm^2 values.

(ii) *Detector length.*—A large detector length increases an experiment's ability to resolve oscillations with position in addition to spectral distortions in energy. This effect can increase overall sensitivity at most Δm^2 values while extending the range of high sensitivity to lower values of Δm^2.

(iii) *Detector-reactor distance.*—The closest reactor-detector distance $r_{\min}$ determines the Δm^2 range of highest sensitivity. To achieve optimized sensitivity $r_{\min}$ should be paired with a detector length d of equal or larger magnitude to allow sampling of a large fraction of the oscillation period. In addition, statistics naturally increase as $r_{\min}$ is decreased.

(iv) *Detector resolution.*—Oscillations at higher Δm^2 are only visible if resolutions and bin sizing are smaller than the oscillation itself. Sensitivity to values of Δm^2 approaching this threshold are significantly reduced.

(v) *Background.*—Understanding backgrounds will be critical for the success of the experiment. Small S/B ratios make it difficult to resolve oscillation effects above statistical background fluctuations and uncorrelated background uncertainties. Raising the analysis energy threshold may improve this S/B ratio, but at the expense of low-energy signal statistics and their attendant oscillation sensitivity. For a given S/B, various background spectral shapes have similar impact on the experiment. However, precise knowledge of the backgrounds and their distribution in energy and position are critical for an experiment's sensitivity and for demonstrating the observation of neutrino oscillation.

Other variables, such as core size, shape, and fuel type will not likely drive experimental design at most mass splittings.

B. Energy versus energy + position measurements

Two classes of detectors have been proposed for very-short-baseline measurements at reactors. The first consists of m^3-sized experiments that will look for oscillation-related distortions in the reactor $\bar{\nu}_e$ energy spectrum. The second class is larger multi-m^3 experiments with good energy and position resolution that are sensitive to both oscillations in position and energy. The sensitivity of these two types of experiments can be compared using the default detector-reactor arrangement for each case while varying the total detector length: the energy-only experiment is defined to have a 1 m detector length, while the energy + position experiment is defined to have a 3 m detector length. A comparison of the sensitivities of three configurations is given in Fig. 18: a 3 m detector with good position and energy resolution, a 1 m detector with good position and energy resolution, and a 1 m detector with no position reconstruction.
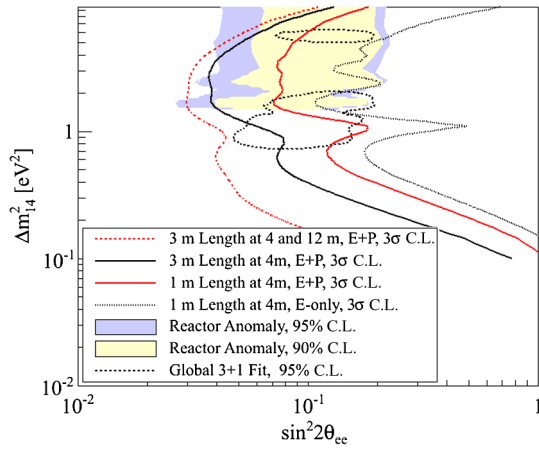
FIG. 18 (color online). Comparison of sensitivities for oscillation experiments with energy-only or energy + position information. All experimental parameters, including closest reactor-detector distance, are identical, except the total detector length. Also pictured is an experiment utilizing an additional similar detector at a longer baseline of 12 m. This extra detector greatly increases the available range of baselines, significantly increasing the experimental sensitivity at lower Δm^2 values.

Experiments with energy + position information provide significantly better sensitivity to oscillations than energy-only experiments. Observing distortions of the energy spectrum at multiple baselines will lessen the effect of uncertainties in the energy spectrum shape. If viewed at a single baseline, an energy spectrum distortion can be more easily described without oscillations by nuisance parameters for individual energy bins. This problem is amplified if oscillations occur at high energies, where the reactor spectral uncertainties are larger. In contrast, distortions from oscillation occur at different energy values for different baselines, an effect not easily neutralized with the comparatively rigid energy spectrum uncertainty nuisance parameters. Large differences also exist between experiments utilizing energy + position information in 1 m and

3 m-long detectors. In addition to the difference in statistics, the 1 m detector samples a shorter portion of the oscillation period as discussed in Sec. V B. Even better sensitivity is achieved by an experiment with multiple detectors, for example at distances of 4 and 12 m, as shown Fig. 18.

IX. CONCLUSION

New experiments at very short distances from reactors have the potential to make a precision measurement of the reactor antineutrino spectrum, resolve the reactor anomaly, and probe a large fraction of the sterile neutrino oscillation parameter space. This paper explores the experimental variables of a short-baseline reactor experiment and resulting experimental sensitivity. The reactor power, detector length, reactor-detector distance, energy and position resolutions of the detectors, signal-to-background ratio, and overall background shape uncertainties are all key parameters for such an experiment.

Radially extended detectors with good position and energy resolution provide a systematically robust approach to the search for neutrino oscillations at very short baselines. A highly extended (>5 m) detector or multiple detectors at different baselines may expand the sensitivity of the experiment to all relevant regions of Δm^2. Furthermore, the use of movable detectors would allow deployment at multiple radial locations, which may mitigate the possible effects of spatially varying backgrounds and will clearly demonstrate the effect of neutrino oscillations.

ACKNOWLEDGMENTS

[1] T. Mueller *et al.*, Phys. Rev. C **83**, 054615 (2011).
[2] K. Abazajian *et al.*, arXiv:1204.5379.
[3] A. Hayes, in Proceedings of the Applied Antineutrino Physics Workshop 2012, Honolulu (unpublished), http://www.phys.hawaii.edu/~jgl/AAP/AAP_2012_Agenda.htm.
[4] P. Huber, Phys. Rev. C **84**, 024617 (2011).
[5] M. Fallot *et al.*, Phys. Rev. Lett. **109**, 202504 (2012).
[6] G. Mention, M. Fechner, T. Lasserre, T. A. Mueller, D. Lhuillier, M. Cribier, and A. Letourneau, Phys. Rev. D **83**, 073006 (2011).
[7] C. Giunti and M. Laveder, Phys. Rev. D **84**, 093006 (2011).
[8] A. Aguilar *et al.* (LSND Collaboration), Phys. Rev. D **64**, 112007 (2001).
[9] A. A. Aguilar-Arevalo *et al.* (MiniBooNE Collaboration), Phys. Rev. Lett. **103**, 111801 (2009).
[10] A. A. Aguilar-Arevalo *et al.* (MiniBooNE Collaboration), Phys. Rev. Lett. **105**, 181801 (2010).
[11] A. A. Aguilar-Arevalo *et al.* (MiniBooNE Collaboration), arXiv:1207.4809.
[12] C. Giunti and M. Laveder, Mod. Phys. Lett. A **22**, 2499 (2007).
[13] C. Giunti and M. Laveder, Phys. Rev. C **83**, 065504 (2011).

[14] E. Komatsu *et al.*, Astrophys. J. Suppl. Ser. **192,** 18 (2011).

[15] J. Hamann, S. Hannestad, J. Lesgourgues, C. Rampf, and Y. Y. Y. Wong, J. Cosmol. Astropart. Phys. 07 (2010) 022.

[16] F. An (Daya Bay Collaboration), Phys. Rev. Lett. **108,** 171803 (2012).

[17] Y. Abe (Double Chooz Collaboration), Phys. Rev. Lett. **108,** 131801 (2012); Phys. Rev. D **86,** 052008 (2012).

[18] J. Ahn *et al.* (RENO Collaboration), Phys. Rev. Lett. **108,** 191802 (2012).

[19] K. M. Heeger, in Proceedings of Neutrino 2012, Kyoto, Japan (unpublished), http://neu2012.kek.jp/neu2012/programme.html.

[20] T. Lasserre, in Proceedings of CIPANP 2012, St. Petersburg (unpublished), http://cipanp2012.triumf.ca/timetable.html.

[21] N. Bowden, in Proceedings of SNAC 2011, Blacksburg (unpublished), http://www.cpe.vt.edu/snac/program.html.

[22] A. Serebrov *et al.*, arXiv:1205.2955.

[23] A. V. Derbin *et al.*, arXiv:1204.2449.

[24] V. Kopeikin, L. A. Mikaelyan, and V. V. Sinev, Phys. At. Nucl. **67,** 1892 (2004).

[25] Y. Abe (Double Chooz Collaboration), Phys. Rev. D **87,** 011102 (2013).

[26] M. Vivier, in Proceedings of the Applied Antineutrino Physics Workshop, Honolulu (unpublished), http://www.phys.hawaii.edu/~jgl/AAP/AAP_2012_Agenda.htm.

[27] N. Bowden *et al.*, arXiv:physics/0612152.

[28] Oak Ridge National Laboratory, The High Flux Isotope Reactor at Oak Ridge National Laboratory, http://neutrons.ornl.gov/facilities/HFIR.

[29] National Institute of Standards and Technology, NIST Center for Neutron Research, http://www.ncnr.nist.gov.

[30] Idaho National Laboratory, Advanced Test Reactor: Meeting US Nuclear Energy Research Challenges, http://www.inl.gov/research/advanced-test-reactor-research.

[31] H. Kwon, F. Boehm, A. Hahn, H. Henrikson, J. Vuilleumier, J. Cavaignac, D. Koang, B. Vignon, F. Feilitzsch, and R. Mössbauer, Phys. Rev. D **24,** 1097 (1981).

[32] San Onofre Nuclear Generating Station, http://www.songscommunity.com/default.asp?from=SONGS.

[33] V. Kopeikin, L. A. Mikaelyan, and V. V. Sinev, Phys. At. Nucl. **69,** 185 (2006).

[34] B. Littlejohn, Ph.D. thesis, University of Wisconsin–Madison, 2012.

[35] S. Abe *et al.* (KamLAND Collaboration), Phys. Rev. Lett. **100,** 221803 (2008).

[36] B. Ackhar *et al.*, Nucl. Phys. B **434,** 503 (1995).

[37] A. Afonin *et al.*, JETP Lett. **54,** 253 (1991).

[38] A. Afonin *et al.*, JETP Lett. **45,** 247 (1987).

[39] NIST Center for Neutron Research, 2012 Operations Schedule, http://www.ncnr.nist.gov/ns_schedule.html.

[40] Oak Ridge National Laboratory, HFIR Operating Forecast & Planning Schedule, http://neutrons.ornl.gov/facilities/HFIR/pdf/rolling15month.pdf.

[41] ATR National Scientific Users Facility, FY 2009 Advanced Test Reactor National Scientific User Facility Users' Guide, https://secure.inl.gov/atrproposal/documents/ATRUsersGuide.pdf.

[42] T. Lasserre (private communication).

[43] F. An (Daya Bay Collaboration), arXiv:hep-ex/0701029.

[44] F. An (Daya Bay Collaboration), Nucl. Instrum. Methods Phys. Res., Sect. A **685,** 78 (2012).

[45] J. Beringer *et al.* (Particle Data Group), Phys. Rev. D **86,** 010001 (2012).

[46] San Onofre Nuclear Generating Station, Anatomy of a Nuclear Power Plant Planned Outage.

[47] R. T. Ridenoure, Docket No. 50-361 60-day Post Cycle-15 Refueling Outage Reactor Pressure Vessel Head Inspection Report for San Onofre Nuclear Generating Station, Unit 2, http://pbadupws.nrc.gov/docs/ML0808/ML080850059.pdf.

[48] D. Ridikas, G. Fioni, P. Goberis, O. Deruelle, M. Fadil, F. Marie, and S. Rottger, On the Fuel Cycle and Neutron Fluxes of the High Flux Reactor at ILL Grenoble, http://cdsweb.cern.ch/record/540488/files/sis-2002-086.pdf.

[49] A. Glaser, Ph.D. thesis, Technical University of Darmstadt, 2005.

[50] P. Vogel and J. Engel, Phys. Rev. D **39,** 3378 (1989).

[51] K. Schreckenbach, G. Colvin, W. Gelletly, and F. Von Feilitzsch, Phys. Lett. B **160,** 325 (1985).

[52] A. Hahn, K. Schreckenbach, W. Gelletly, F. von Feilitzsch, G. Colvin, and B. Krusche, Phys. Lett. B **218,** 365 (1989).

[53] C. Lewis (private communication).

[54] F. Boehm *et al.* (Palo Verde Collaboration), Phys. Rev. D **64,** 112001 (2001).

[55] J. C. Anjos, in Proceedings of the Applied Antineutrino Physics Workshop, Honolulu (unpublished), http://www.phys.hawaii.edu/~jgl/AAP/AAP_2012_Agenda.htm.

[56] M. Yeh (private communication).

[57] A. Glenn (private communication).

[58] C. D. Bass *et al.*, arXiv:1206.4036.

[59] F. Seukane, in Proceedings of the Applied Antineutrino Physics Workshop, Honolulu (unpublished), http://www.phys.hawaii.edu/~jgl/AAP/AAP_2012_Agenda.htm.